Available online at www.eccomasproceedia.org
Eccomas Proceedia COMPDYN (2017) 2119-2137

ECCOMAS
Proceedia

COMPDYN 2017
6th ECCOMAS Thematic Conference on
Computational Methods in Structural Dynamics and Earthquake Engineering
M. Papadrakakis, M. Fragiadakis (eds.)
Rhodes Island, Greece, 15–17 June 2017

SEISMIC RESPONSES OF REGULAR HIGHWAY BRIDGES UNDER NEAR-FAULT GROUND MOTIONS (COMPDYN 2017)

Hai-Bin Ma[1], Wei-Dong Zhuo[1], Gabriele Fiorentino[2], Davide Lavorato[2], Camillo Nuti[2], Ying Sun[1]

[1] Civil Engineering College, Fuzhou University
Xueyuan Road No.2 ,University Town, Fuzhou City, Fujian Province
e-mail: {m140510011, zhuowd, sunying}@fzu.edu.cnz

[2] Architecture Department, Roma Tre University
Largo Giovanni Battista Marzi, 10, 00153 Roma
{gabriele.fiorentino, davide.lavorato, camillo.nuti }@uniroma3.it

Keywords: Near-fault, Regular Highway Bridge, SDOF, Makris Model, Spectrum Analysis, Seismic Analysis.

Abstract. *Ground motions recorded in near-fault areas have some specific characteristics that differ substantially from those recorded in far-fault regions. One of the main features of near-fault records is the pulse-like shape caused by forward-directivity effect. This peculiarity may lead to much more severe damage to bridge structures located in near-fault regions. However, both current Chinese and European codes for seismic design of highway bridges nearly have no consideration on near-fault seismic actions. In this study, typical regular highway bridges in China are idealized as single-degree-of-freedom (SDOF) systems. Then, the Makris mathematical model for the pulse-like records is used to perform a parametric analysis on a settled SDOF system. Effect of key parameters, such as the half-pulse number (n), fundamental period (T_0), pulse period (T_p) and the peak velocity (V_p) from the mathematical model, on responses of SDOF systems are analyzed. The potential degradation phenomenon which might happen under near-fault earthquake ground motions is also considered by comparing the ductility coefficient spectrum. The results show that all the key parameters had a significant effect on both linear and nonlinear response spectrum and seismic response. The stiffness degradation phenomenon will lead to a larger ductility*

Peer-review under responsibility of the organizing committee of COMPDYN 2017.
doi: 10.7712/120117.5554.18034

coefficient and the Vp is the most effective factor for the response under the near-fault mathematical input.

1 INTRODUCTION

Near-fault (NF) ground motions recorded in recent major earthquakes (1994 Northridge, 1999 Chi-Chi, 2008 Wenchuan and 2016 Central Italy earthquake) exhibit significant pulse in their velocity time histories. According to the literature there are mainly two phenomena which can cause pulse-like records: rupture directivity and fling-step. Rupture directivity effect usually happens when the fault rupture propagates towards the site with a velocity close to the shear velocity V_S [1], and it typically shows an intense double-side pulse in the velocity time history at the recording site. Fling-step is the permanent static displacement caused by tectonic offset characterized with a single-sided velocity pulse, so that integration results in a permanent offset in the displacement time history [2]. In comparison with the ordinary earthquake records, the NF pulse-like records concentrate most of energy in a narrow frequency band and can lead to larger elastic spectral demands especially for structures with periods close to the velocity pulse period [3][4]. The pulse features also lead to more severe inelastic demands to the SDOF system [5][6]. These observations highlight the importance to study structures subjected to NF pulse-like ground motions.

In this regard, researchers presented a series of mathematical models for the NF pulse-like record to remedy to the lack of original earthquake records. These mathematical models can not only represent the main effect of the NF pulse-like models, but also establish a predictive relationship with the key parameters extracted from the ground motion. Although with different expression form, the most widely used models can be divided into 3 types:

- Type I - The simple function type. Somerville [7] first identified the pulse as impact to analyze its effects on structures, a regression formula composed by a factor of pulse period, pulse peak value, magnitude and fault distance is put forward. On this basis, Krawinkler and Alavi [8] improved the expression as P2 style model with the rectangle acceleration shape; the expression model can represent the significant response character of NF pulse-like records according to the analysis results. Jennings [9] modified the pulse effect with a linear function to get an analytical solution on the SDOF system in the elastic case and the results showed that the largest displacement may not happen when structural period is equal to pulse period, but the structure can show larger responses at lower frequencies.
- Type II - The trigonometric function type. Makris [10] categorized the NF pulses into 3 different trigonometric functions of different periods; this combination could provide an ideal result to modify the main component of the NF pulse-like records. Xin-le [11] compared some existing models for near-fault velocity pulses and proposed an improved one on the base of the formula presented by Makris.
- Type III - The exponential function type. Menun and Fu [12] proposed a five-parameter model consisting of exponential and sine functions, for any

specified near-fault record it could be established by nonlinear regression method. He and Agrawal [13] improved the model by expressing the shape of secondary half pulse thus obtaining a more complex form of the mathematical model which has new parameters.

In this paper, as an alternative to current approaches, Makris mathematical model is used to modify the main pulse component choosing as key parameters the half-pulse number (n), the pulse period (T_p) and the peak velocity (V_p). Aiming at the regular highway bridges, Clough hysteretic model is used to build the nonlinear behavior of the pier. Sensitivity analysis is performed both in the elastic and inelastic case, the interactions between the key parameters are compared by means of orthogonal experiment design method, and the distribution map of displacement and acceleration for the SDOF system is provided and discussed.

2 SDOF MODELLING AND MAKRIS MODEL

Based on the samples statistics of the Chinese seismic design code [14], a 3-span continuous bridge is selected to build the representative model for SDOF system (Fig.1-a). Focusing on the longitudinal direction, the bridge can be characterized by the response of a single pier with a frame of continuous girder on its top. The fixed pier is formed by a 1.2 m diameter circular column adopts 0.8% reinforcement and 0.7% transverse reinforcement. The yield and ultimate moment-curve relationships are calculated on the designed parameter by XTRACT [15], then the Clough model is chosen to modify the nonlinear hysteric behavior of the pier.

The Makris mathematical model used a 3-parameter trigonometric function form (n, T_p and V_p). Usually these parameters are extracted from natural ground motion records. However, without the consideration of the high frequency component of the earthquake records, there can be a large difference between the mathematical model spectrum and original earthquake record spectrum for short period structures.

Based on the NF pulse-like shape, the record from Northridge earthquake recorded in Newhall site is selected as the simulation basis; the least square regression method is used to get the minimum spectrum difference with the consideration of the most representative period range for bridge structures, then the key parameters extracted are set as: n=2, T_p=1.5s and V_p=90 cm/s. Eq.1 and Eq.2 show the velocity and acceleration time history expressions where w_p is the frequency parameter relevant with the pulse period.

$$V(t) = -V_p \sin w_p t \tag{1}$$

$$A(t) = -V_p w_p \cos(w_p t) \tag{2}$$

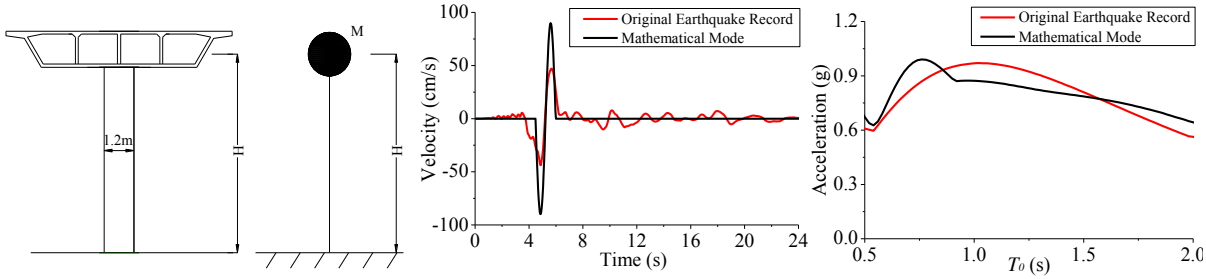

(a): The SDOF system (b): Velocity time history (c): Acceleration spectrum

Fig 1: The modified SDOF system and the Makris input.

According to Fig.1-b the generated mathematical model can provide a good effect to modify the main component of the velocity pulse. Fig.1-c shows the comparison between acceleration spectra of both pulse-like records at 5% damping ratio. The difference between the spectra is acceptable for the analysis.

2 ELASTIC SPECTRUM ANALYSIS

The response spectrum is an important tool for expressing the excitation response relationship between earthquake engineering and seismic design. In order to capture the salient response features of pulses, several studies have examined the response spectra of single-pulse or separate pulse [16][17], but a systematic analysis of the pulse parameters has not been performed.

2.1 General solution to the dynamic equation

After the mathematical model and SDOF system are set up, the general solution to the dynamic equation can be solved with a two-part solution. The first part is the homogeneous solution for the equation as $\bar{u}(t)$ and the second part is the particular solution as $u^*(t)$.

$$\ddot{u}(t)+2\xi w_0\dot{u}(t)+w_0^2u(t)=-Vw_p\cos(w_pt)=\ddot{u}_g(t) \quad (0,T_p) \tag{3}$$

$$u(t)=\bar{u}(t)+u^*(t) \tag{4}$$

For the first part, set $\bar{u}(t)=Ce^{\lambda t}$ for the homogeneous solution, Eq.3 can be written as:

$$\lambda^2+2\xi w_0\lambda+w_0^2=0 \tag{5}$$

Based on Eq.5 the parameter λ can be solved as:

$$\lambda=w_0(-\xi\pm\sqrt{\xi^2-1}) \tag{6}$$

Set $w_d=w_0\sqrt{1-\xi^2}$, under low damping condition the Eq.5 can be expressed as:

$$\lambda=-\xi w_0\pm iw_d \tag{7}$$

Therefore, the final homogeneous solution for $\bar{u}(t)$ is the expression in Eq.8

$$\bar{u}(t) = e^{-\xi w_0 t}(A_1 \cos w_d t + A_2 \sin w_d t) \tag{8}$$

For the second part, the particular solution can be set as the Eq.9 base on the formula.

$$u^*(t) = B_1 \cos w_p t + B_2 \sin w_p t \tag{9}$$

Combined with Eq.3 The Eq.9 can be transformed

$$(-B_1 w_p{}^2 + 2w_p \xi w_0 B_2 + B_1 w_0{}^2 + V w_p)\cos w_p t + (-B_2 w_p{}^2 - 2B_1 \xi w_o w_p + B_2 w_0{}^2)\sin w_p t = 0 \tag{10}$$

Set $(-B_1 w_p{}^2 + 2w_p \xi w_0 B_2 + B_1 w_0{}^2 + V w_p) = 0$ and $-B_2 w_p{}^2 - 2B_1 \xi w_o w_p + B_2 w_0{}^2 = 0$

The solution for B_1 and B_2 is can be expressed as follows where $u_{st} = \dfrac{V\beta}{w_0}$ and $\beta = \dfrac{w_p}{w_0}$

$$B_1 = -u_{st} \cdot \frac{1-\beta^2}{(1-\beta^2)^2 + (2\xi\beta)^2} \; ; \quad B_2 = -u_{st} \cdot \frac{2\xi\beta}{(1-\beta^2)^2 + (2\xi\beta)^2}$$

With the initial statement of the SDOF system ($u_{first} = 0$, $\dot{u}_{first} = 0$), the solution for A_1 and A_2 can also be solved.

$$A_1 = -C = -u_{st} \cdot \frac{\beta^2 - 1}{(1-\beta^2)^2 + (2\xi\beta)^2} \; , \quad A_2 = -(C\xi + D\beta) = u_{st} \cdot \frac{\xi(1+\beta^2)}{(1-\beta^2)^2 + (2\xi\beta)^2} \tag{11}$$

Above all, the displacement response for the SDOF system under the chosen mathematical model can be expressed as Eq.11

$$u(t) = e^{-\xi w_0 t}(A_1 \cos w_0 t + A_2 \sin w_0 t) + C \cos w_p t + D \sin w_p t \tag{12}$$

The acceleration response for the SDOF system can be obtained by deriving twice the expression of u(t).

$$\ddot{u}(t) = w_0{}^2 e^{-\xi w_0 t}[(\xi^2 A_2 + 2\xi A_1 - A_2)\sin w_0 t + (\xi^2 A_1 - 2\xi A_2 - A_1)\cos w_0 t] - w_p{}^2 (C \cos w_p t + D \sin w_p t) \tag{13}$$

2.2 Sensitivity analysis

(1) Half-pulse number effect (*n*)

Even for the typically NF earthquake event, the half-pulse number has a certain randomness. Based on the summary statistics for the typical NF pulse-like records, commonly half-pulse numbers range from 1 to 3 [18]. Makris model mainly considers values of 1 or 2 for the half-pulse number which correspond to the fling-step effect and the rupture directivity effect. According to the mathematical model assumption the half-pulse number effect is analyzed. Fig.2 (a) shows the acceleration time-history input, the related NF effect is used to describe the relevant half-pulse number effect.

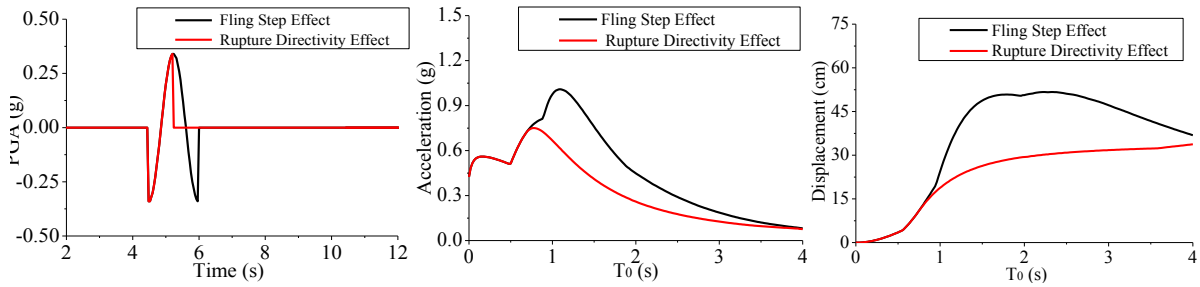

(a) Acceleration input (b) Acceleration spectrum (c) Displacement spectrum

Fig 2: The comparison between the mathematical models of different half-pulse number.

Fig.2(b) and Fib.2(c) show the response spectrum of the mathematical models for different half-pulse numbers, the rupture directivity effect acquired a higher value both in acceleration and displacement spectrum. When compared to the fling-step, the rupture directivity can make the acceleration spectrum acquire the largest value at a longer period and lead displacement spectrum with a decrease section of pulse-like shape. Both the results show that the largest response may not happen at the same period of the pulse; this trend is also consistent with the Jenning`s former research conclusions [9].

(2) Peak velocity effect (V_p)

In the Makris mathematical model, both V_p and T_p will influence the input acceleration directly according to Eq.2. For this case, one parameter should be established as a first invariant during the analysis. During the V_p effect analysis T_p is assumed to be fixed at 1s based on the original earthquake records. V_p ranges from 30cm/s to 180 cm/s at a spacing of 30cm/s with the number V_{p1}~V_{p6}, as a consequence the PGA for the input ranges from 0.13g to 0.77g as depicted in Fig.3(a).

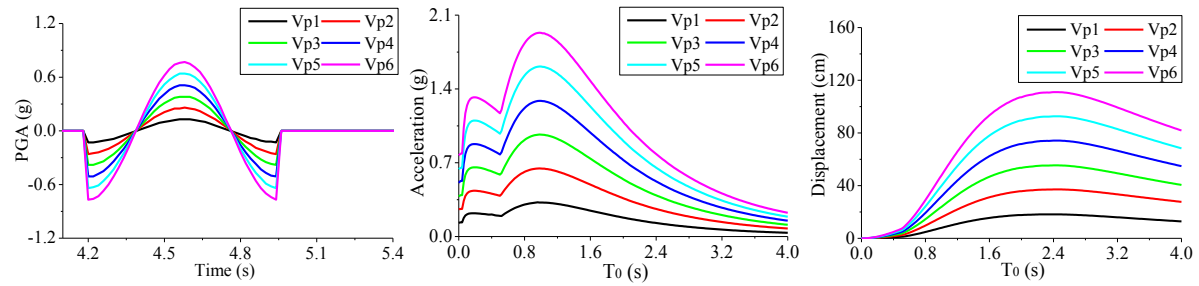

(a) Acceleration input (b) Acceleration spectrum (c) Displacement spectrum

Fig 3: The comparison between the mathematical models of different peak velocity value.

Fig.3 (b) and (c) showed the effect of V_p on the response spectrum. The peak spectrum value follows a linear correlation based on the uniform distribution with the V_p spacing. As the V_p changes, the peak acceleration spectrum value increases from 0.33g to 1.93g and the peak displacement spectrum value increases from 18.19 cm to 110.99 cm which indicates severe damage to the structures.

(3) Pulse Period effect (T_p)

T_p is another important parameter for mathematical models; in Makris model it influences not only the peak value of acceleration but also a very important intensity measure value which is PGV/PGA. Liao first point out that PGV/PGA>0.2 can be a representative character of the NF pulse-like records [19]. However, in Makris model the PGV/PGA ratio can be obtained as function of T_p as described in Eq.14.

$$PGV / PGA = V_p / V_p w = T_p / 2\pi \tag{14}$$

To analyze the T_p influence, an initial V_p value of 75cm/s is set as a constant. While T_p is ranging from 1s to 3.5s at a spacing of 0.5s, the PGV/PGA ranges from 0.16s to0.56s at a spacing of 0.08s and the PGA for the input ranges from 0.56 to0.16g as depicted in Fig.4 (a).

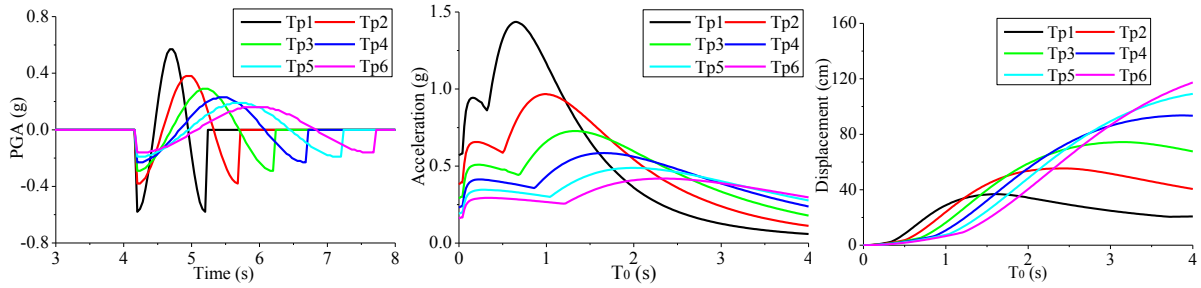

(a) Acceleration time history (b) Acceleration spectrum (c) Displacement spectrum

Fig 4: The comparison between the mathematical models of different pulse period.

Fig.4 (b) and (c) show the T_p effect on the response spectrum. The peak value of the displacement spectrum increases with the spacing T_p however the peak value of the acceleration spectrum shows a decreasing trend; the peak value of the spectrum is not consistent with the pulse period. Although the PGA for the input decreases, the spectrum still gets a larger value during the longer period part and also a larger displacement response; this effect will increase the seismic demand especially for long-period structures.

2.3 Comparison with Seismic Design Code

The standard response spectrum in current design code is based on a vast calculation of original earthquake records with the combination of engineering experience. UBC-97 was the first seismic design code to take into account this special kind of seismic records. In fact, with the near-source factor C_a and C_v coordinate with the site condition, spectrum shape can be changed to adjust the NF earthquake [20]. The current Chinese seismic design code and Eurocode 8 are mainly based on the elastic spectrum design theories which focus on far-field earthquake records. On this basis some researchers proposed optimized methods to adjust the special effect of the NF earthquake. One of the representative methods proposed by Xu is to enlarge the platform segment for long period structures and modify the maximum spectrum value according to the regression from the records [21]. In order to compare the main spectrum caused by the NF pulse-like record, we selected 50 records from PEER earthquake

data base with significant velocity pulses [22]. NSPECTRA, a software developed by Buffalo University, is used to calculate the mean spectrum value to compare with seismic design code spectrum [23].

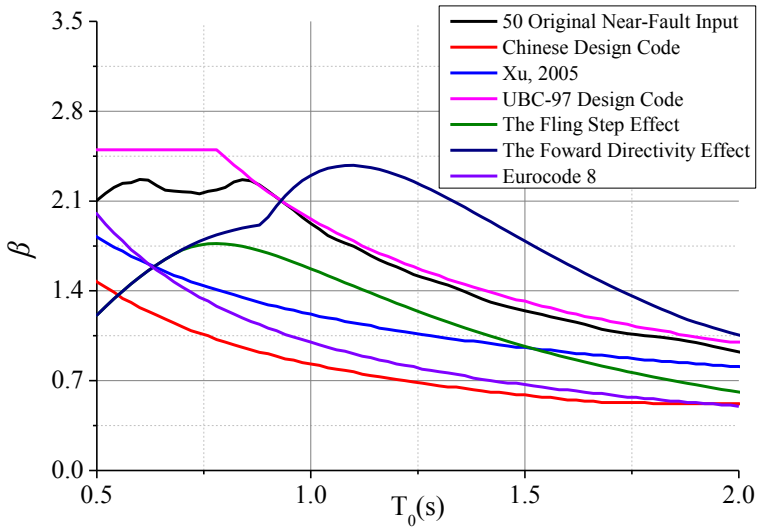

Fig 5: The spectrum comparison between the mathematical models and different design codes of Chinese Design Code, UBC-97 Design Code, Eurocode8 and Xu`s improved design code.

Based on the comparison UBC-97 can provide a higher seismic security with β_{max} value at 2.5 however the Chinese design code spectrum is relatively low at a β_{max} value of 2.25. The peak spectrum of fling-step effect is lower than the UBC-97 design value and the rupture directivity effect lead to a value larger than all design code spectra values; the Eurocode 8 can provide a better consideration when compared with Chinese Design Code however is still limited for the NF effect; the mean value of original records acquires a larger long-period component around 1s as the rupture directivity effect spectrum. Xu`s improved design spectrum considers long-period structures but is still not capable to cover the original records spectrum. With the definition of the near-source factor, UBC-97 can provide a good requirement for the NF earthquake.

3 INELASTIC SPECTRUM ANALYSIS

Because of the limited amount of natural NF pulse-like records, structures have an inelastic behavior which can cause damage due to the lack of appropriate design. Chopra`s research proved that the equation for the ductility still can be used during the NF seismic event. the nonlinear response spectrum can be divided into 2 types: the constant-ductility strength demand spectrum and the constant-strength ductility spectrum. With the chosen parameters in NSPECTRA, the constant-strength ductility spectrum is selected with different values of the strength reduction factor. According to Chopra`s definition, the strength reduction factor R_y is defined as the ratio between yield force f_y and the maximum force f_0 of the elastic case, the ductility coefficient μ is the ratio between the maximum inelastic displacement u_m and the yield displacement u_y, the u_0 is the maximum displacement of the elastic case [24]. Then the

ductility coefficient μ can be deduced as described in Eq 15 and Eq 16.

$$R_y = \frac{f_0}{f_y} = \frac{u_0}{u_y}, \quad \mu = \frac{u_m}{u_y}, \quad \frac{u_m}{u_0} = \mu \bar{f}_y = \frac{\mu}{R_y} \tag{15}$$

$$\mu = \frac{u_m}{u_0} R_y \tag{16}$$

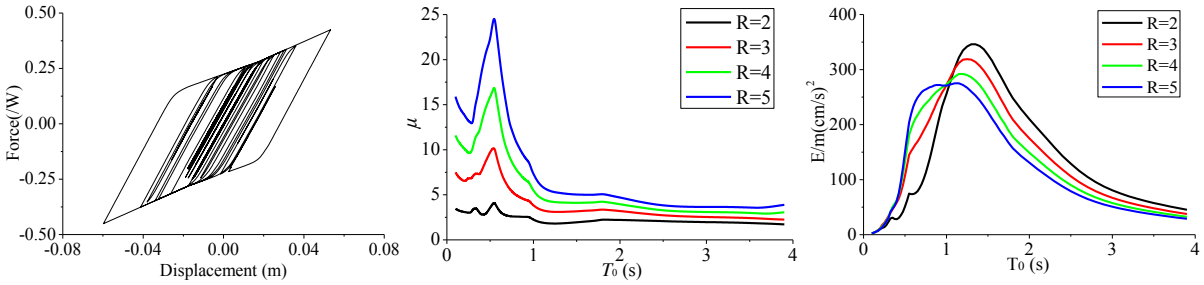

(a) Clough hysteric model (b) Nonlinear spectrum (c) Input energy spectrum

Fig 6: The hysteric model for the SDOF and the nonlinear response spectrum.

Fig.6 (a) shows the hysteretic behavior under El Centro earthquake record（1940，N-S）. The hysteretic force is scaled with the ratio of mass. The Nonlinear spectrum depending on different values of the strength reduction factor is depicted in Fig.6 (b). The ductility coefficient rises as the strength reduction factor grows and the ductility coefficient spectrum still has a pulse-like shape as the elastic spectrum. When the structure period is longer than the pulse period (T_p=1s) the ductility coefficient spectrum has an almost constant part when compared with the short-period part. The input energy for the NF pulse-like records is defined as the sum of the kinetic energy, the damping energy and the hysteretic energy, the predominant spectrum period becomes shorter as the reduction factor increases as in Fig.6 (c).

3.1 Effect of parameters on the inelastic spectrum

(1) Effect of the variation of the half-pulse number (n)

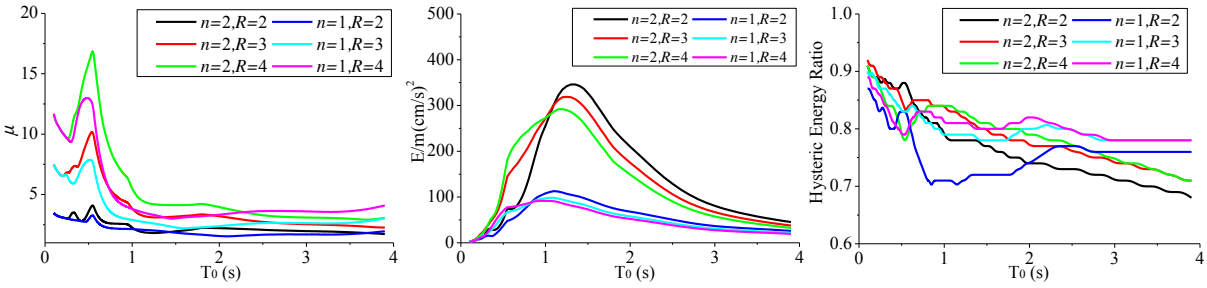

(a) *Nonlinear spectrum* (b) Input energy spectrum (c) Hysteric energy ratio spectrum

Fig 7: The nonlinear response spectrum under half-pulse number effect.

In this section the variability of the spectra depending on the half-pulse numbers is described. The nonlinear spectrum for values of the strength reduction factor R of 2, 3 and 4 is

evaluated (Fig.7). The ductility coefficient spectrum and the input energy spectrum show a pulse-like shape distribution and the predominant period is similar to the different R level. If the ductility spectra for different values of n (n=1, n=2) are compared, it is possible to point out that the peak μ value is quite similar for R=2 for the different half-pulse numbers, while the difference grows as the value of R increases. By making the same comparison for the hysteretic energy ratio spectrum, it can be observed that it shows an overall decreasing tendency, while during the long period the single-pulse input acquires a higher hysteretic energy ratio.

(2) Peak velocity effect (V_p)

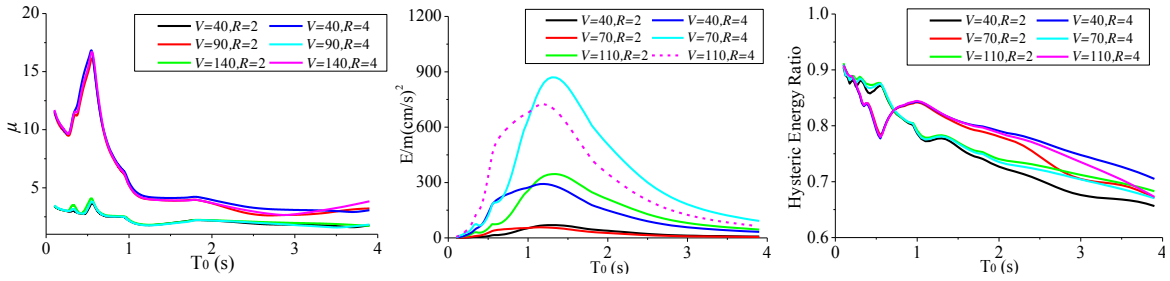

(a) Nonlinear spectrum (b) Input energy spectrum (c) Hysteric energy ratio spectrum

Fig 8: The nonlinear response spectrum under V_p effect.

The nonlinear ductility spectra at a peak velocity of 40 cm/s, 70 cm/s and 110 cm/s are calculated with a fixed value of T_p based on the mathematical background. According to the distribution for different R values, V_p has a significant impact on the input energy, however there is a weak influence on the ductility spectrum and the hysteretic energy ratio spectrum, the influence of V_p is more significant with longer structure period and stronger strength ductility factor.

(3) Pulse period effect (T_p)

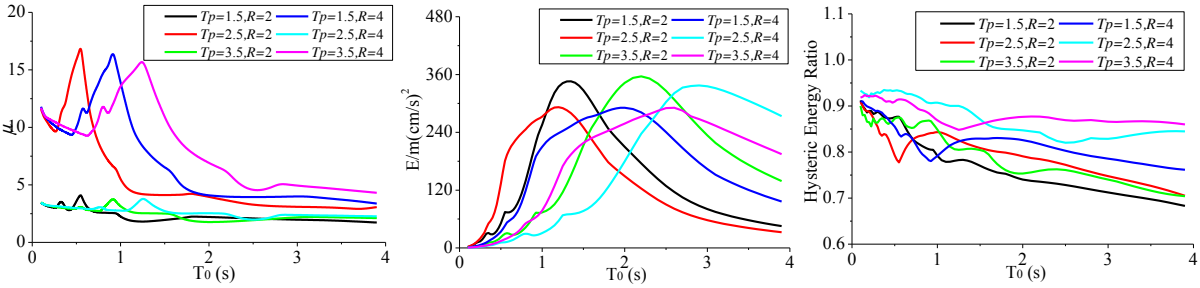

(a) Nonlinear spectrum (b) Input energy spectrum (c) Hysteric energy ratio spectrum

Fig 9: The nonlinear response spectrums under T_p effect.

Based on the mathematical background, the nonlinear ductility spectra at a pulse period of 2s, 3s and 4s are calculated with fixed value of peak velocity. According to the distribution

depicted in Fig.9, T_p has a more significant effect on the nonlinear spectrum than V_p . For the same value of R, the maximum value of μ remains almost constant while the predominant period and input energy gets larger as T_p increases; the hysteretic energy ratio has a decreasing tendency as T_0 grows, for all values of T_p.

3.2 Different hysteric model effect

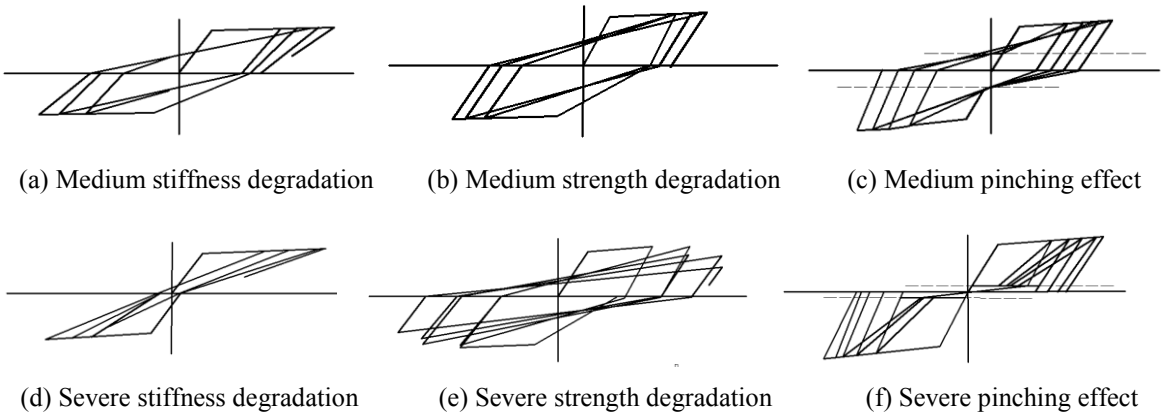

(a) Medium stiffness degradation (b) Medium strength degradation (c) Medium pinching effect

(d) Severe stiffness degradation (e) Severe strength degradation (f) Severe pinching effect

Fig 10: Different hysteretic model for degradation and pinching.

During the NF strong ground motion the attenuation of the earthquake energy is not remarkable due to the short transmission distance. This fact can cause stiffness degradation, strength degradation and pinching effect for the inelastic behavior. By modifying the degradation parameters in NSPECTRA presetting, the different hysteretic models for degradation and pinching can be expressed. For the sake of simplicity, the comparison is carried on in the cases of non-degradation, medium and severe degradation in accordance with degradation parameters in NSPECTRA presetting.

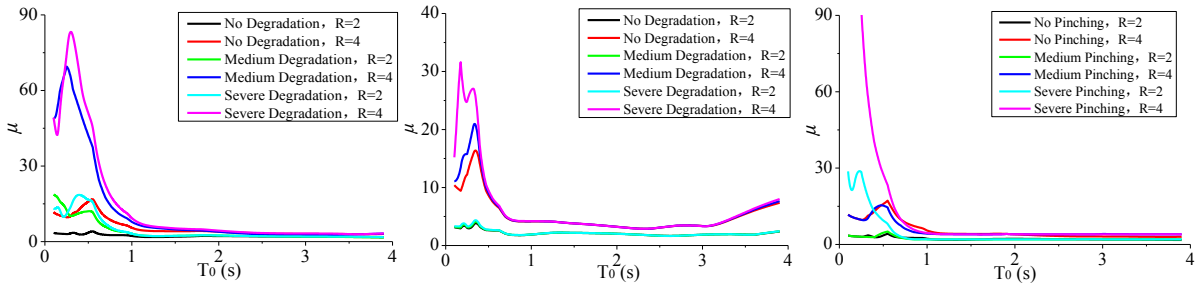

(a) Stiffness Degradation (b) Strength Degradation (c)Pinching Effect

Fig 11: The nonlinear spectrum for different hysteric models.

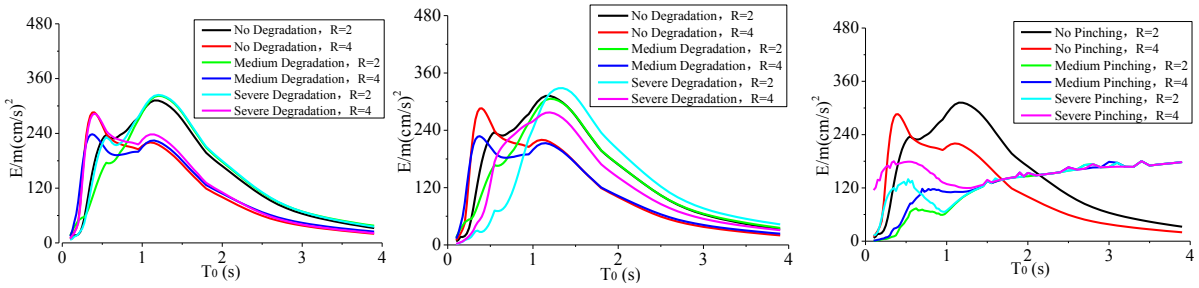

(a) Stiffness Degradation (b) Strength Degradation (c)Pinching Effect

Fig 12: The input energy spectrum for different hysteric models.

The Nonlinear spectrum and the input energy spectrum for different degradation hysteretic model are listed in the Fig.11 and Fig.12. According to the distribution results, pinching effect and stiffness degradation are the most significant effects for the maximum value of the ductility coefficient; strength degradation effect on ductility coefficient is relatively lower but it cannot be neglected. The input energy for stiffness degradation and strength degradation remains similar with a pulse-like shape, however the input energy has a tendency to increase in pinching effect during the long structure period.

4 SEISMIC RESPONSE ANALYSIS

The response spectrum represents a convenient tool which summarizes the peak response of all possible SDOF systems to a particular ground motion. However, it also neglects some important information contained in the response time history, which are valuable for structural design analysis. Therefore, it is necessary to examine the waveform characteristics of the response time histories of the SDOF system subjected to the excitation of these special types of pulses. During the sensitivity analysis for the peak time history values, the V_P is assumed ranging from 15cm/s~300cm/s with a spacing of 15cm/s and T_p ranging from 0.5s~10s with a spacing of 0.5s based on the Northridge mathematical model.

(a) Peak Velocity Effect (V_p)

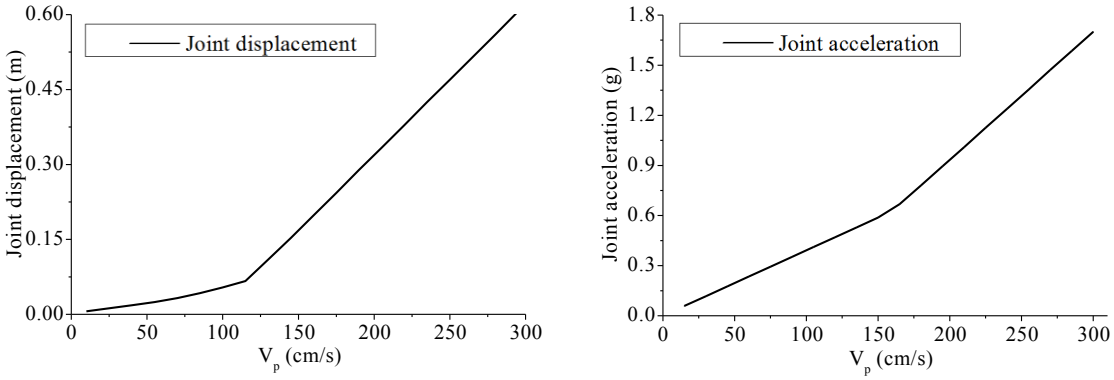

(a) Joint displacement (b) Joint acceleration

Fig.13 Peak value for the time-history result under V_P effect.

As the PGA value increases as the V_P grows from the Makris mathematical model, the peak value for the SDOF time-history response follows a linear increase tendency both for acceleration and displacement. The joint displacement increases from 0.02m to 0.60m and the joint acceleration increases from 0.06g to 1.70g significantly as V_P ranges from 10cm/s to 300cm/s which indicates the direct linear effect of V_P on structures according to the Makris mathematical model.

(b) Pulse Period Effect (T_p)

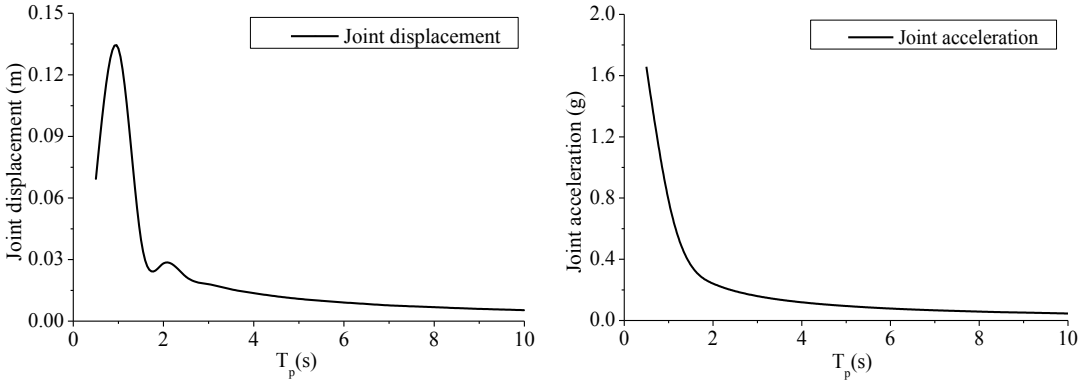

(a) Joint displacement (b) Joint acceleration

Fig 14: Peak value for the time-history result under T_P effect.

Fig.14 shows the distribution of the peak SDOF reaction with the increased T_P. The joint displacement follows a complex sine function form and the joint acceleration follows an exponential distribution. During the elastic case the two components of the analytic solution discussed in Eq.11 have different dominant pulse periods, while the peak displacement appears at the pulse period for T_p=1s. The joint displacement acquires the maximum value of 0.13m at the pulse period of 1s as the joint acceleration decreases from 1.68g to 0.05g.

5 THE INTERACTION ANALYSIS

With the exception of the direct effect on the SDOF seismic response of key parameters from the mathematical model, the interactions between the key parameters haven been often neglected in past studies. In order to investigate these interactions, orthogonal experimental design method is used to compare the key parameters. T_0, V_p and T_p are selected as the base factors and a sensitivity analysis is done by choosing 3-level value with uniform spacing for each parameter. The proposed factor and level details are listed in Tab.1, then the orthogonal form L_{27} (3^{11}) can be selected to carry out the calculation by 27 samples of parameters at different levels. To avoid the mix of advanced interactions in this work, we only consider the primary interactions (Tab.2).

There are two steps for analyzing the results: range analysis and variance analysis. The range analysis assumes that when focusing on one impact of the factor, the influence of other factors on result is balanced. Tthe variance analysis is used to estimate the relative significance of each parameter in terms of contribution percentage to the overall response.

This paper does not present the calculation processes of mean and range, the details of which can be found in [25].

For the range analysis, it consider the values of T_i, R and $\overline{x}_i$, the T_i data is obtained by summing the drift ratio of factors at the same level, R is the value for each factor calculated by finding the difference between the maximum and minimum values, $\overline{x}_i$ is the average value of T_i base on the calculation time and the T is the summation of all values. For example, if levels for focused factor are assumed as A, B and C for each factor in L_{27} (3^{11}) the calculation time is 9, then the $\overline{x}_i$ value can be calculated as Eq 17.

$$\overline{x}_i = (A_1+A_2+A_3+\ldots+A_9)/9 \tag{17}$$

For the variance analysis, it considers the sum of squares, degrees of freedom, F variance ratio, F standard value and the significance where *SS* represent the summation of the squares, *df* represent the freedom degree, *MS* represent the average sum of squares and *F* represent the significance indicator [25]. The F standard value is determined from an F-table for a given statistical level of significance. If the F variance ratio ranks higher than the F standard value, the corresponding factor will have significant contributions to the overall results. The tables for various significance levels and different degrees of freedom are available in most handbooks [26].

Factor / Level	Fundamental period T_0 (s)	Pulse Velocity V_p (cm/s)	Pulse Period T_p (s)
1	1	100	3
2	2	200	6
3	3	300	9

Tab 1: The selected factor at different levels.

Number	1	2	3	4	5	6	7	8	9	10	11	12	13
Factors	T_0	V_p	$T_0\times V_p$		T_p	$T_0\times T_p$		$V_p\times T_p$		Vacancy			

Tab 2: The Label details for the $L_{27}(3^{11})$ experiment design.

Tab.3 and Tab.4 show the range and variance analysis for the calculation of joint acceleration response, where the T_i is the summation results of the data at same level, T is the sum of all 27 results of the experiment, $\overline{x}_i$ is the mean value of the same level results, R_j is the maximum difference value of $\overline{x}_i$, *SS* is the sum of the squares, *df* the degree of freedom, *MS* the average sum of squares and *F* is the significance indicator.

According to the range and variance analysis for the joint displacement, T_0 and V_p are the most significant factors according to the significance indicator value when compared with the F distribution for $\alpha = 0.1$; $T_0\times V_p$ is the strongest interaction with the significance indicator value larger than F distribution at α =0.1; The other interactions are not so strong based on the joint displacement data. Tab.5 and Tab.6 show the range and variance analysis for the calculation of joint acceleration response. When compared with the joint displacement, the acceleration data can provide a better evaluation with a larger significance indicator F value.

Indicator	Effect factors					
	T_0	V_p	$T_0 \times V_p$	T_p	$T_0 \times T_p$	$V_p \times T_p$
T_1	7.81	5.97	12.31	8.03	10.79	11.11
T_2	1.59	10.09	10.63	1.26	12.04	11.22
T_3	13.05	15.10	8.90	11.60	8.20	9.57
$\overline{x_1}$	0.87	0.66	1.37	0.89	1.20	1.23
$\overline{x_2}$	1.18	1.12	1.18	1.36	1.34	1.25
$\overline{x_3}$	1.50	1.68	0.99	1.29	0.95	1.06
R_j	0.63	1.01	0.37	0.47	0.39	0.18
						T=31.9

Tab 3: Displacement range analytical data: summation of the data at same level, maximum difference value and the average value of summation.

Indicator	*SS*	*df*	*MS*	*F*	Significance
T_0	1.799	2	0.8995	8.076	**
V_p	3.983	2	1.9915	17.881	**
$T_0 \times V_p$	1.445	4	0.36125	3.243	*
T_p	1.115	2	0.5575	5.163	*
$T_0 \times T_p$	0.745	4	0.18625	1.672	
$V_p \times T_p$	0.532	4	0.133	1.194	
Deviation	0.89	8			
	$F_{0.05}(2, 8)=19.37$,	$F_{0.1}(2, 8)=9.37$,	$F_{0.25}(2,8)=3.35$		
	$F_{0.05}(4, 8)=6.04$,	$F_{0.1}(4, 8)=3.95$,	$F_{0.25}(4, 8)=2.08$		

Tab 4: Displacement variance analytical data: summation of the squares, freedom degree, average sum of squares and significance indicator.

Index	Effect Parameters for the sensitivity analysis					
	T_0	V_p	$T_0 \times V_p$	T_p	$T_0 \times T_p$	$V_p \times T_p$
T_1	2.27	0.86	1.68	2.43	1.98	1.62
T_2	1.69	1.77	1.72	1.65	1.77	1.70
T_3	1.33	2.59	1.90	1.22	1.45	1.98
$\overline{x_1}$	0.25	0.10	0.19	0.27	0.22	0.18
$\overline{x_2}$	0.19	0.20	0.19	0.18	0.20	0.19
$\overline{x_3}$	0.15	0.29	0.21	0.14	0.16	0.22
R_j	0.10	0.19	0.02	0.13	0.06	0.04
						T=5.29

Tab 5: Acceleration range analytical data: summation of the data at same level, maximum difference value and the average value of summation.

Indicator	*SS*	*df*	*MS*	*F*	Significance
T_0	0.050	2	0.0250	25.0	***
V_p	0.153	2	0.0765	76.5	***
$T_0 \times V_p$	0.003	4	0.0008	1.50	
T_p	0.083	2	0.0415	41.5	***
$T_0 \times T_p$	0.021	4	0.0053	5.25	**
$V_p \times T_p$	0.017	4	0.0043	4.25	**
Deviation	0.010	8			
	$F_{0.05}(2, 8)=19.37$,	$F_{0.1}(2, 8)=9.37$,	$F_{0.25}(2,8)=3.35$		
	$F_{0.05}(4, 8)=6.04$,	$F_{0.1}(4, 8)=3.95$,	$F_{0.25}(4, 8)=2.08$		

Tab 6: Acceleration variance analytical data: summation of the squares, freedom degree, average sum of squares and significance indicator..

Based on the range analysis, the order of significance of the parameters which influence the SDOF joint acceleration response is $V_p > T_p > T_0 > T_0 \times T_p > V_p \times T_p > T_0 \times V_p$. The significance analysis for both displacement and acceleration provides similar results. When comparing the effect of a single parameter, the influence of interactions is relatively low. Among the interaction effect, $T_0 \times V_p$ is the weakest and the significance value is less than the F critical value for α=0.25; the interaction between the $T_0 \times T_p$ and $V_p \times T_p$ is relatively strong with the significance value larger than the F critical value for α=0.1. Therefore, the interaction between the $T_0 \times T_p$ and $V_p \times T_p$ cannot be neglected during the analysis for the SDOF acceleration. The joint acceleration response allows better evaluating the influence of interactions and the order of significance of parameters in comparison with joint displacement response.

6 OVERALL DISTRIBUTION ASSESSMENT

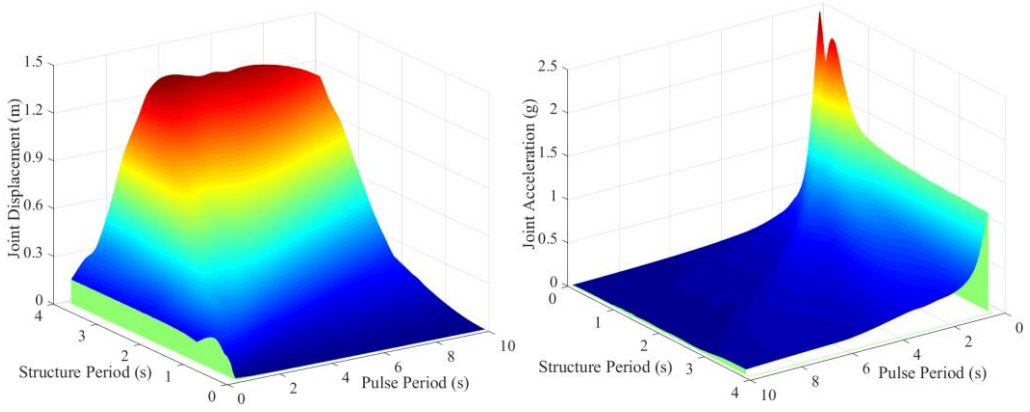

Fig 15: The overall displacement and acceleration distribution map.

After the conclusion that V_p has a linear effect on the structural response, for a further comprehensive assessment, the overall displacement and acceleration distribution map are listed in the Fig.15 with variable T_p and T_0. The calculation result is based on T_p ranging from

1s to 10s at a spacing of 1s and T_0 ranging from 0.1s to 10s with a spacing of 0.1s. According to the distribution T_0/T_p is still an important parameter for structural response, there is a crest both in the displacement and acceleration distribution map that divides the diagram into two parts. The displacement response is larger in Makris model with longer structurl period while the acceleration reaction increases with a smaller structural period, both results are affected by the ratio T_0/T_p.

7 CONCLUSIONS

- The Makris mathematical model provides a good modification effect to NF pulse-like records; the analytical solution can be deduced by the dynamic equation for a SDOF system.
- The key parameters from the mathematical model can affect the seismic response of the SDOF system both for elastic and inelastic behavior. Factor n and V_p follow a positive correlation tendency while the effect of T_p is accompanied with sin-geometry and exponential form to the joint displacement and acceleration.
- Except the single factor effect, the interaction between the parameter factors cannot be neglected. The interaction between $T_0 \times T_p$ and $V_p \times T_p$ are quite significant.
- The comprehensive function assessment for 3 typical SDOF systems are presented with the joint displacement and acceleration, the distribution map can be used for engineering seismic response analysis.
- The number of SDOF samples and mathematical models can be expanded in the next step of the research for a more accurate evaluation result.

REFERENCES

[1] Somerville, PG, N F Smith, R W Graves, et al. Modification of empirical strong ground attenuation relations to include the amplitude and duration effects of rupture directivity. *Seismological Research Letters*, 1997, 68(1):199-222.

[2] Bolt B, Abrahamson N. Estimation of strong seismic ground motion. *International Geophysics*, 2003, 81:983-1001.

[3] Ambraseys, N. N. & Douglas, J. Near-field horizontal and vertical earthquake ground motions. S*oil Dynamics and Earthquake Engineering*, 2003, 23(1):1-18.

[4] Manitakis, C. A. & Spyrakos, C. C. 2012. A new methodology to determine elastic displacement spectra in the near-fault region. *Soil Dynamics and Earthquake Engineering*, 2011, 35(2):41-58.

[5] Mavroeidis, G. P., Dong, G. & Papageorgiou, A. S. Near-fault ground motions, and the response of elastic and inelastic single-degree-of-freedom (SDOF) systems. *Earthquake Engineering & Structural Dynamics*, 2004, 33(33):1023-1049.

[6] Tong, M., Rzhevsky, V., Dai, J., et al. Near-fault ground motions with prominent acceleration pulses: pulse characteristics and ductility demand. *Earthquake Engineering*

and Engineering Vibration, 2007, 6(3):215-223.

[7] Somerville PG. Magnitude scaling of the near fault rupture directivity pulse. *Physics of the Earth and Planetary Interiors*. 2003, 137(1–4):201-212.

[8] Krawinkler H, Alavi B. Development of an improved design procedure for near-fault ground motions. *SMIP 98 seminar on utilization of strong motion data*, Oakland, CA, 1998.

[9] Jeanings P C. Ground motion pulses and structural response. *Frontiers in the New Millennium*, Spencer and Hu (eds), 2001:119-125.

[10] Makris N. Rigidity-plasticity-viscosity: can electrorheological dampers protect base-isolated structures from near-source ground motions. E*arthquake Engineering & Structure Dynamitic*, 1997, 26(5): 571-591.

[11] Li Xinle, Dou Huijuan, Sun Jiangang. Sensitivity parameters analysis of bridge seismic response for near-fault simple velocity pulse ground motion. *Journal of Dalian Nationalities University*. 2008, 16(3):261-265.

[12] Menun C．Qiang F．An analytical model for near-fault ground motions and the response of SDOF systems．*Seventh U S National Conference on Earthquake Engineering*．Boston．Massachusetts．Mira Digital Publishing．2002．No．00011．

[13]He, W.L. and Agrawal, A.K. A Closed-Form Approximation of Near-Fault Ground Motio n Pulses For Flexible Structures. Proceedings of 2002 ASCE Engineering Mechanics Con ference, Columbia University, New York, July 2002.

[14] JTG/T B02-01-2008. Guidelines for seismic design of highway bridges. Beijing: People's Communications Press (Chinese Edition).

[15] C. B. Chadwell, R. A. Imbsen. XTRACT: A Tool for Axial Force - Ultimate Curvature Interactions[C]. *Structures Congress 2004*. May 22-26, 2004 | Nashville, Tennessee, United States.

[16] Chopra, A. K. & Chintanapakdee, C. 2001. Comparing response of SDF systems to near-fault and far-fault earthquake motions in the context of spectral regions. *Earthquake Engineering & Structural Dynamics*, 2001, 30(12):1769-1789.

[17] S Yaghmaei-Sabegh，N Jalali-Milani. 2012. Pounding force response spectrum for near-field and far-field earthquakes. *Scientia Iranica*, 2012, 19(5):1236–1250.

[18] Jiang Hui. Performance-Based seismic design of bridge structure excited by near-fault earthquake using energy concept. Ph.D. Thesis. College of Civil Engineering, Beijing Jiaotong University, 2007.

[19] Liao, W.-I., Loh, C.-H. & Lee, B.-H. Comparison of dynamic response of isolated and non-isolated continuous girder bridges subjected to near-fault ground motions. *Engineering Structures*, 2004, 26(14):2173-2183.

[20] UBC-97 Uniform Building Code. *International Conference of Building Official*,1997.

[21] Xu Longjun, Xie Lili. Study on seismic design spectra of near-fault region. *Journal of Southeast University (Natural Science Edition)*. 2005, 35(Sup I):105-108.

[22] PEER, available from URL: http://peer.berkeley.edu/smcat/search.html. Accessed December 2013.

[23] NSPECTRA. A Program for Response Spectra of Nonlinear and Linear Systems, available from URL: http://civil.eng.buffalo.edu/nspectra/

[24] Chopra. *Dynamics of Structures: Theory and applications to earthquake engineering (Second Edition)*. Higher Education Press, 2007.

[25] Wirier BJ, Brown DR, Michels KM. Statistical principles in experimental design. New York: McGraw-Hill: 1971.

[26] Cogkun S, Motorcu AR, Yamankaradeniz N, Pulat G. Evaluation of control parameters' effects on system performance with Taguchi method in waste heat recovery application using mechanical heat pump. Int J Refrig 2012;35(4):795-809.